Exciton effects in perovskite nanocrystals

Journal of Physics: Photonics

CrossMark

OPEN ACCESS

RECEIVED
15 December 2020

REVISED
8 February 2021

ACCEPTED FOR PUBLICATION
11 March 2021

PUBLISHED
8 April 2021

PERSPECTIVE

Exciton effects in perovskite nanocrystals

Ruben Ahumada-Lazo[1,5], Rinku Saran[2,5], Oliver Woolland[3], Yunpeng Jia[3], Maria-Eleni Kyriazi[4], Antonios G Kanaras[4], David Binks[1] and Richard J Curry[3,*]

[1] Department of Physics and Astronomy, Photon Science Institute, University of Manchester, Manchester M13 9PL, United Kingdom
[2] School of Electrical and Computer Engineering, University of Oklahoma, Norman, OK 73019, United States of America
[3] Department of Electrical and Electronic Engineering, Photon Science Institute, University of Manchester, Manchester M13 9PL, United Kingdom
[4] School of Physics and Astronomy, Faculty of Engineering and Physical Sciences, University of Southampton, Highfield, Southampton SO17 1BJ, United Kingdom
[5] These authors contributed equally.
[*] Author to whom any correspondence should be addressed.

E-mail: richard.curry@manchester.ac.uk

Keywords: perovskite nanocrystal, excitonic effects, energy transfer, Rashba effect, superfluorescence, polariton lasing, single photon emission

Abstract

Nanocrystals (NCs) of perovskite materials have recently attracted great research interest because of their outstanding properties for optoelectronic applications, as evidenced by the increasing number of publications on laboratory scale devices. However, in order to achieve the commercial realisation of these devices, an in-depth understanding of the charge dynamics and photo-physics in these novel materials is required. These dynamics are affected by material composition but also by their size and morphology due to quantum confinement effects. Advances in synthesis methods have allowed nanostructures to be produced with enhanced confinement and structural stability, enhancing the efficiency of energy funnelling and radiative recombination and so resulting in more efficient light emitting devices. In addition, photovoltaics could greatly benefit from the exploitation of these materials not only through their deployment in tandem cell architectures but from the use of multiple exciton generation in these NCs. These systems also offer the opportunity to study quantum effects relating to interactions of excited states within and between NCs. Properties and behaviour that includes an enhanced Rashba effect, superfluorescence, polariton lasing, Rydberg exciton polariton condensates, and antibunched single photon emission have been observed in a single metal halide perovskite NC. The further study of these in NC systems will shed new light on the fundamental nature of their excited states, their control and exploitation. In this perspective, we give an overview of these effects and provide an outlook for the future of perovskite NCs and their devices.

1. Introduction

Metal halide perovskites (MHPs) are a family of materials with the general formula ABX_3, where A can be an organic cation, like methylammonium (MA, $CH_3NH_3^+$) and formamidinium (FA, $CH(NH_2)_2^+$) or a large inorganic cation like caesium (Cs^+), B is a divalent cation (most commonly lead (Pb^{2+}) but can be substituted by Sn^{2+}, Ge^{2+} or other metallic ions for a lead-free compositions) and X is a halide ion, such as Cl^-, Br^- and I^- (or the mixture of two of these with similar radii) [1–3]. Although these materials have been known for decades, their development as nanocrystals (NCs) has recently attracted significant research interest due to their excellent properties for optoelectronic applications [4–7]. These include high charge carrier mobilities, long carrier diffusion lengths, and narrowband emission with photoluminescence quantum yields (PLQYs) close to 100% that can be tuned across the entire visible spectra (as well as into the UV and near infrared) by altering the chemical composition and morphology [7]. A wide range of perovskite NC-based optoelectronic devices have been fabricated and tested at the lab scale with remarkable results [7–10]. However, further improvements in efficiency and stability are needed before full commercial

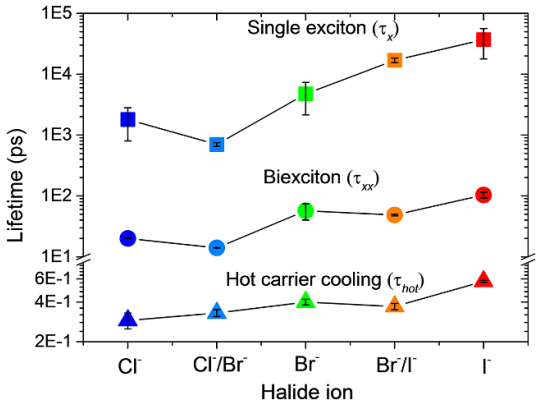

Figure 1. Single exciton lifetime (τ_x), biexciton lifetime (τ_{xx}) and hot carrier cooling time (τ_{hot}) as a function of halide ion in all-inorganic $CsPbX_3$ perovskite nanocrystals. Data compiled from multiple references by Mondal *et al* [11].

realisation of these applications is reached. This requires in-depth understanding of the fundamental photo-physics and the dynamics of charges within the perovskites and also with various interfaces [11]. In this perspective, we first discuss recent advances in two novel aspects of exciton dynamics in perovskite NCs that have been only briefly covered in a previous review [2] and are of particular relevance to enhanced performance in optoelectronic devices. These are: (a) multiple exciton generation (MEG), also known as carrier multiplication, which has the potential to increase the efficiency of solar cells, and (b) energy funnelling, which can be used to improve the efficiency of light emitting devices. Then we discuss exciton-phonon interactions including the observation of bright triplet states and studies of exciton linewidths and anomalous bandgap shifts. Finally, we consider emission schemes and emission phenomena including up and down conversion, polariton lasing and single photon emission.

2. Novel aspects of exciton dynamics

2.1. Charge dynamics in MHP; effects of composition and quantum confinement

The charge dynamics in and at the interfaces of photoactive materials have a key influence on the efficiency of optoelectronic devices. Therefore, understanding these phenomena is fundamental to the optimization of materials and structures which will eventually result in commercial MHP-based devices. Ultrafast pump-probe spectroscopic techniques allow the monitoring of photoinduced processes at a wide range of energies and with very high time resolution. Although the studies of charge dynamics in perovskites had mainly focused on bulk materials or thin films in the past, the development of perovskite NCs by Protesescu *et al* [5] and the first comprehensive work by Makarov *et al* [12] were followed by many publications on ultrafast dynamics and optoelectronic properties in NCs of various morphologies and compositions [7, 11]. In general, perovskites show composition dependent properties, e.g. the band gap and exciton binding energies decrease, while the recombination lifetimes of single excitons, biexcitons, and trions as well as the carrier trapping and hot carrier cooling times become longer, as the halide anion (which mainly effects the valence band) changes from Cl^-, to Br^- and to I^- (see figure 1) [11]. Moreover, the carrier cooling time also increases as the strength of the carrier–phonon interaction decreases with changes in the *A* site cation, from FA to MA and then to Cs [13]. Exciton dynamics in MHP NCs are also affected by quantum confinement effects as they are in other semiconductors and the rates of radiative and non-radiative recombination mechanisms are size dependent [14]. However, most MHP NCs, which are cubically shaped with side lengths of a few nanometres, are in the weak confinement regime because of their small Bohr radii, which range from 2.5 nm to 6 nm in all-inorganic compositions and from 1.3 nm to 5 nm in the hybrid counterparts [2, 5]. Consequently, biexciton Auger lifetimes have been observed to scale linearly with volume for small NCs, in agreement with the well-known 'universal volume scaling' but deviate to sub-linear scaling for larger NCs [15]. These large NCs generally present more bulk-like properties and can therefore be regarded as 3D NCs [16]. However, through modifications in the synthesis, it is possible to limit their growth in one or two directions to produce 2D nanoplatelets/nanosheets (NPs/NSs) [16, 17] and 1D nanowires with enhanced confinement, i.e. blue shifted absorption/emission and exciton binding energies significantly larger than in bulk materials and 3D NCs [16, 18]. Although, strongly confined 0D MHP colloidal NCs (where all dimensions are smaller than the Bohr radius) with high PLQY were initially unstable and difficult to produce [19], modifications to the synthesis and passivation methods have recently resulted in stable and monodisperse symmetric NCs with dimensions down to 3–4 nm [20, 21]. In addition,

low-dimensional-networked (low-DN) perovskites are emerging alternatives offering superior confinement and the possibility of novel compositions [22].

2.2. Multiple exciton generation (MEG)

MEG is the process by which the excess energy of hot carriers photogenerated by the absorption of a photon with energy at least twice the band gap ($h\nu_{th} = 2E_g$) can be used to create additional electron–hole pairs instead of being dissipated through thermalisation [23–28]. This effect has the potential to boost the photocurrent of photovoltaic devices, allowing the Shockley–Queisser efficiency limit to be overcome [29]. Although it has been demonstrated in a number of semiconductor materials (with moderate efficiencies) and is believed to be enhanced by different effects accompanying quantum confinement (e.g. strengthened Coulomb interactions, relaxation of momentum conservation, enhanced Auger processes and modified cooling rates [23, 24]), its exact mechanism is not yet fully understood and different theoretical descriptions have been proposed [30]. As photovoltaic devices are one of the most promising applications of halide perovskites [31] and given the significant research interest raised by their development as NCs, the emergence of studies looking for MEG in MHP NCs is not surprising. The first attempt to detect MEG used transient photoluminescence measurements with an excitation energy 2.65 times the band gap (1.82 eV) in cubic $CsPbI_3$ NCs (edge length ~11.2 nm) [12]. However, the fast Auger decay and higher occupancy of the excited state that would indicate the presence of multiple excitons produced by MEG were not seen in that study. These observations were explained by an argument based on classical mechanics where, given that the effective masses of electrons and holes in these perovskites are very similar ($m_e \approx m_h$), the excess photon energy is equally divided between both carriers, which increases the threshold energy to $\sim 3E_g$ according to $h\nu_{th} = E_g\left(2 + \frac{m_e}{m_h}\right)$ [32]. More recently, low energy thresholds of $\sim 2.25E_g$ and MEG efficiencies of 75% and 50% were reported for $FAPbI_3$ NCs with sizes of 7.5 nm and 9.8 nm, respectively [33]. These high efficiencies were attributed to slow carrier cooling (two times longer than in the bulk counterpart) being outcompeted by the faster (~90 fs) MEG, which is an inverse Auger process. Moreover, they argue that small and similar electron and hole effective masses and the intermediate confinement in these NCs, are favourable for slowing the carrier cooling (phonon bottleneck) [34] and help reconcile the contrasting effects of enhanced Coulomb coupling and reduced density of states in the strong confinement regime. In addition, the authors demonstrated a power conversion efficiency (PCE) calculation based on the detailed balance equation showing that assuming a 100% MEG efficiency and under AM 1.5 illumination, the peak PCE can be improved to above 40% for energy thresholds close to $2E_g$. In another study published in the same volume [35], a very high MEG efficiency of 98% was observed in weakly confined $CsPbI_3$ NCs (11.5 ± 0.6 nm) using an excitation energy of $\sim 2.4E_g$. In that work, the authors use independent experimental approaches (showing an additional fast component in the transient absorption dynamics, photon energy dependence of carrier generation yield in the linear regime of excitation fluence and photo-bleach rise times) to corroborate their results. These examples show that MEG commences at excitation energies just above the energy conservation limit ($2E_g$) rather than $\sim 3E_g$, indicating that a quantum mechanical approach is needed to accurately predict the threshold. MEG was also shown to not be an instantaneous process, where the hot carrier losing energy by the process is not transferred directly to the lowest state and the additional carriers appear after those initially generated upon photon absorption in a state with longer cooling time. At the time of writing, the latest study of MEG in perovskites [36] reports efficiencies exceeding 90% and 40% for strongly (6.2 nm) and weakly (12.1 nm) confined $CsPbI_3$ NCs, respectively. Analysing the hot carrier cooling and ground state bleach dynamics, the authors observed that although the cooling times are similar for both sizes of NCs, the initial hot carrier temperature is two times higher and the Auger recombination is four times slower in the larger NCs. They concluded that there is no photon bottleneck in quantum confined $CsPbI_3$ NCs and that enhanced Coulomb coupling and relaxed momentum conservation are more likely responsible for the higher MEG efficiency in smaller, more confined NCs. Although some of these studies on MEG in perovskite NCs present contrasting results, all of them shed some light into the carrier multiplication mechanism, and since this is still an emerging field of study, it is expected that new research will start to unveil the full picture over time.

2.3. Energy funnelling

The ability to control the dimensions of MHP enables the fabrication of mixed phases of 2D and 3D NCs denoted as quasi-2D perovskites (figure 2). In these structures, the *A* site cations can be substituted by organic ligands, separating the corner-sharing BX_6 octahedrons and producing atomically-thin NPs of variable thicknesses (corresponding to a number of monolayers, *n*). These NPs can then be packed into thin films with tuneable orientations on a substrate [37] or self-assembled into a colloid of large cuboid crystals of intercalated perovskite and organic ligand layers as shown in figure 2(b) [38]. The much wider energy

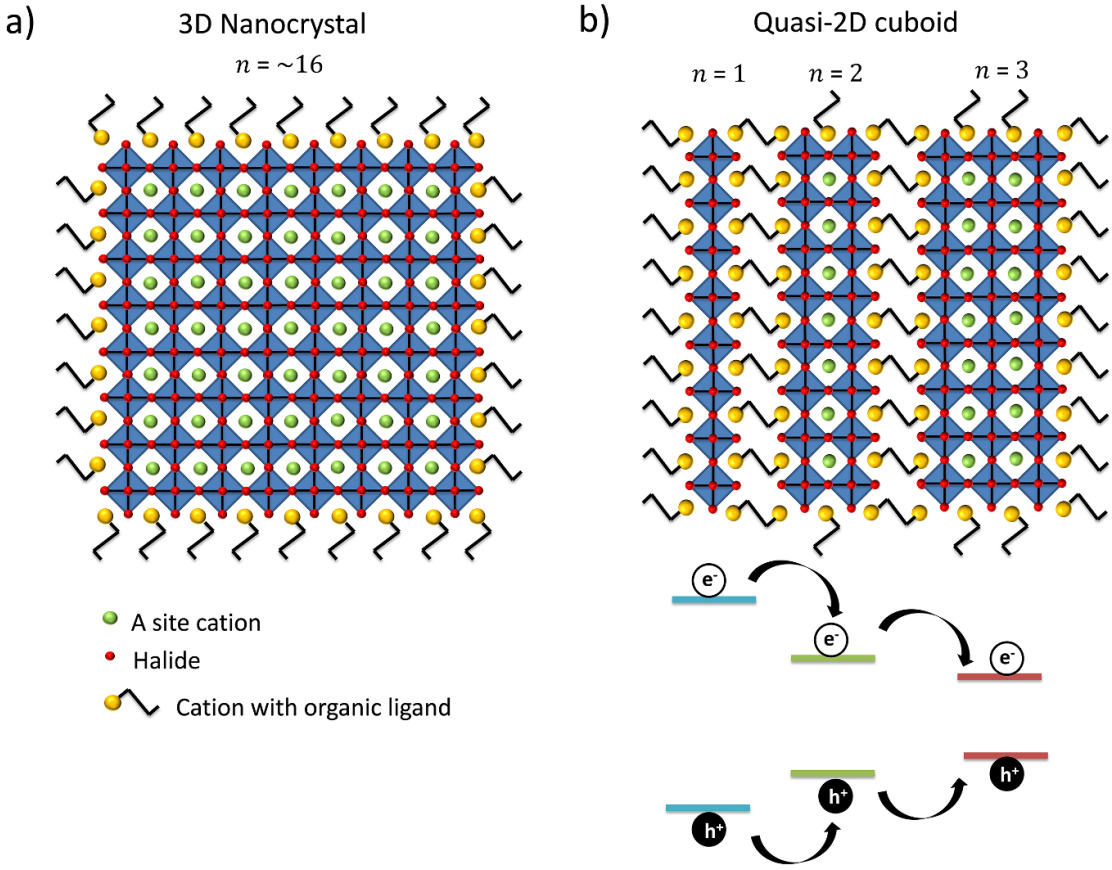

Figure 2. (a) Schematic diagram of a 3D perovskite NC. Typical cubic NCs with ~10 nm side lengths are composed of approximately 16 inorganic layers of corner-sharing BX_6 octahedrons (only eight layers shown in the picture for clarity) with the *A* site cations (this can be organic or inorganic) occupying the spaces created by this framework while the surface is passivated by organic ligands attached to cations. Carriers are subject to weak confinement and have small binding energies. (b) In quasi-2D structures, the organic ligands attached to cations are intercalated between the inorganic layers which assemble in a mixture of domains with different number of layers (n) that determine the energy band gap due to increased confinement of the carriers in the inorganic layers. This increases the exciton binding energy. The energy diagram at the bottom represents the energy funnelling from the high band gap regions ($n = 1$) to the lower band gap regions ($n = 3$) within the structure.

separation of the organic layer's highest occupied molecular orbital and lowest unoccupied molecular orbital compared to the bandgap of the perovskite layer, and their respective difference in dielectric constant, results in materials with quantum well-like electronic properties, where the band gap is determined by the thickness of the perovskite layers [18]. Efficient energy 'funnelling' from the larger band gap regions (thinner NPs) to the smallest band gap region (thicker NPs or 3D NCs), produces charge-carrier localization and high concentrations of carriers in the thick NCs, which results in improved radiative recombination rates and aids in the build-up of population inversions [37, 39]. In addition, surface defects (and specifically halide vacancies) which have been shown to introduce mid-gap trap levels acting as non-radiative recombination centres, are passivated during the ligand-driven self-assembly process, further increasing the PLQY and structural stability [18, 40]. Besides tailored quantum confinement, 2D and quasi-2D perovskites offer the possibility of selecting the organic cation and ligand chains to enhance or inhibit electrical conductivity and to impose hydrophobicity to the surface, increasing the stability against humidity [18]. These advantages make quasi-2D perovskites nanostructures even more promising than 3D NCs for LEDs, photovoltaics, and lasing applications.

3. Exciton fine structure and exciton-phonon interactions

3.1. Bright triplets and the Rashba effect

In organic semiconductors and molecular crystals, the lowest energy exciton states are triplet in nature with non-zero spin. Direct electric-dipole optical transitions from these low-lying energy states are forbidden due to the selection rules and can therefore only proceed with a spin flip of one of the charge carriers. Even if a spin flip process occurs, photon emission from the triplet states is very weak as it relies on the inefficient magnetic-dipole moment associated with the spin coupling. As discussed above under optical excitation high

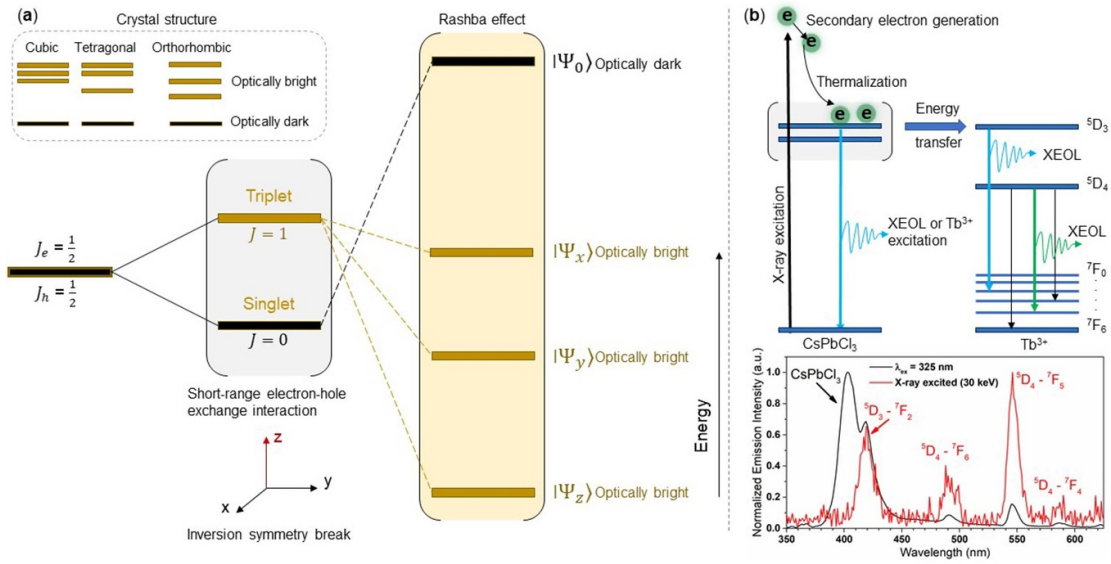

Figure 3. (a) Schematic diagram adapted from [41] of MHP NC excitonic splitting. The singlet ($J = 0$) and triplet ($J = 1$) states (left) are split by the exchange interaction (centre) and then further modified by the Rashba effect (right) yielding three low-lying optically bright states. (b) Schematic of x-ray excitation process leading to XEOL from Tb-doped $CsPbCl_3$ NCs.

PLQY have been reported as these involve excitation and emission from singlet sates. However, electrical excitation via the injection of electrons and holes with random spin results in a ratio of 1:3 for the creation of singlet ($J = 0$) and triple ($J = 1$) excitonic states. This has a direct impact in limiting the efficiency of electroluminescence to 25%, though this can be exceeded if mixing of the singlet and triplet states through spin–orbit (**L.S**) coupling. For inorganic NCs, low-energy excitonic states are analogously referred to as dark excitonic states. The MHP NCs are unusual compared to most other inorganic NCs in displaying bright emission from their lowest energy excitonic state [41]. In these NCs, formation of exciton involves hole in the s-type valence band Coulombically bound to an electron in one of the p-type Pb orbitals. The presence of heavy atom like Pb in their crystal structure causes a strong L.S coupling between the spin and the orbital motion of carrier yielding a doubly degenerate ($J_e = 1/2$) state for electrons. When combined with the s-like hole state ($J_h = 1/2$) the usual exchange interaction results in the singlet and triplet exciton states with the singlet state having the lowest energy (figure 3(a)). Furthermore, and unusually, consideration of the selection rules for optical transitions revealed that the probability of photon emission from the singlet state is zero and non-zero for the triplet states. When the **L.S** coupling is combined with the crystal or inversion symmetry breaking it can give rise to the Rashba effect [42]. The consequence of which is that it reduces the triplet state energy to below the singlet state and further splits the triplet fine structure by lifting the degeneracy of different angular momentum projections ($|x\rangle$, $|y\rangle$ and $|z\rangle$ states), figure 3(a). Optical transitions from all these low energy excitonic states are experimentally observed via the linearly polarized PL spectroscopy at cryogenic temperatures. These excitonic states are not distinguishable at room temperature as they are strongly mixed and the energy difference between these states is only a few meV. However, these bright triplet states have large oscillator strengths which underlies the high PLQY observed, and their fast-radiative lifetimes even at low temperatures relative to other NCs.

It should be noted that this behaviour originates from a combined effect of orthorhombic crystal structure, a strong spin–orbital coupling and the Rashba effect. The exciton fine structure for cubic and tetragonal phases (inset to figure 3(a)) is illustrated in detail elsewhere [43, 44]. Furthermore, as the exchange interaction is governed by the overlap of electron and hole wavefunctions they display a strong dependence on NCs size. For smaller NCs, the exchange interactions are enhanced such that the inversion induced by the Rashba effect is suppressed. Magneto-optical μ-PL on single MHP NCs further revealed that there is a cross-over between the Rashba effect and the Zeeman effect at ≈4 T above which Zeeman splitting of bright exciton dominates and splitting has a linear dependence on applied field [45]. In addition, the Zeeman splitting of bright excitonic states were observed to display a strong anisotropy of the exciton Landé g-factor. Splitting occurs only when their z-axis is oriented parallel to the applied magnetic field providing an exciton g-factor, $g^{ex}\cos\theta = g^{e} + g^{h} \approx 2$. ($\theta$, is the angle between the NCs z-axes and the magnetic field, g^{e} is electron g-factor ≈2 and g^{h} is hole g-factor ≈0.4) [44, 46].

The energetic order of bright sublevels and dark states is still under debate as experimental evidence observed in other perovskite NCs contradicts the inversion of these states which was proposed to explain strong and fast emission at low temperatures. For example, in $FaPbBr_3$ and $CsPbI_3$ NCs the dark exciton state is found lower in energy than the bright state [47, 48]. An alternative interpretation put forwarded is that the presence of a low-lying dark exciton state does not hinder emission from bright states at low temperatures, unlike in NCs of conventional semiconductors. The bright-to-dark spin relaxation is inhibited because the radiative decay from the bright state is much faster than their relaxation to the dark state and the splitting between both states is much larger than the acoustic phonon energy. Interestingly, application of magnetic field can induce coupling between both states enabling bright-to-dark relaxation. The spectroscopic signature of dark exciton emission appears as an additional red-shifted emission with a slow relaxation time providing strong evidence that in these perovskites ground excitonic state is a singlet dark state.

3.2. Exciton linewidth and anomalous bandgap shift

The wide broadening of excitonic linewidth of uniformly sized NCs at room temperature is primarily due to lattice vibrations of the crystal that perturbs the motions of excitons. Such a perturbation can occur via the exciton deformation potential interaction with optical or the acoustic phonons—analogous to a homogenously strained crystal. In crystals lacking centro-symmetry, the electric field induced by the strain can cause exciton interaction with acoustic phonons via the piezoelectric effect. The Coulombic interaction of exciton with longitudinal electric field created by an optical phonon due to displacement of oppositely charged out-of-phase atoms is referred to as the Fröhlich interaction. Since the population of phonons is temperature dependent these interactions vary accordingly and temperature dependent PL spectroscopy (300 K–5 K) can be employed to investigate these interactions [49]. It is revealed that the wide broadening of the excitonic linewidth of $CsPbX_3$ NCs at room temperatures arises due to the strong exciton–phonon coupling. This occurs predominantly via the Fröhlich interaction which is responsible for a broadening of almost twice that resulting from acoustic phonons which dominate only at low temperatures. Similar investigations performed under quasi-resonant excitation (excitation within the PL band of the NCs) and μ-PL on single NC [50, 51] also observed strong Fröhlich interaction, which it found to decrease with the decrease in NC size [52]. Such an interaction can cause a phonon-bottleneck effect [53] by slowing down the hot carrier relaxation and is experimentally verified by two-dimensional electronic spectroscopy [54]. High temperature PL spectroscopy conducted up to 550 K displayed a continuous broadening of the NCs excitonic linewidth with the increase in temperature, accompanied by an increase in PL lifetimes, due to exciton conversion into free charge carriers [55].

Perovskite NCs display an anomalous temperature dependent bandgap shift i.e. their bandgap is found to decrease with the decrease in temperature. Two factors mainly contribute to variation in bandgap with temperature—thermal expansion or contraction of lattice constant and the electron-phonon coupling. The latter depends on the Bose–Einstein phonon occupation number. For $CsPbX_3$ NCs, this behaviour was explained by invoking the Bose–Einstein two-oscillator model [49]. Analysis and modelling of temperature dependent shift of their PL peak position via this model revealed that their bandgap is renormalized due to electron–phonon coupling. The acoustic vibrations accounting for the heavier atomic mass element (Pb) dominates over the lighter atomic mass optical phonon oscillators (halides). This observation is found consistent with the temperature dependent absorption of the NCs [56], though in this study a three-oscillator model was required to fit the data. Additionally, the bandgap renormalization in these NCs is found to have a strong dependence on charge carrier density. The bandgap renormalization constant, that is the amount of bandgap shift as a function of carrier density is calculated $\approx 6.0 \pm 0.3 \times 10^{-8}$ eV cm [57]. Further it is of interest to note that for MAPbI3 perovskites, which also display similar shift of bandgap energy, the thermal expansion component was also found to account for almost 60% of the overall bandgap renormalization [58]. However, relative to bulk crystals and thin films the contribution of thermal expansion component for NCs with diameter of ≈8–4 nm was observed to reduce to ∼25% [59]. This results in the electron–phonon coupling component dominating in these NCs due to enhanced overlap of the strongly confined exciton wavefunction and the NC phonons.

4. Emission schemes and emission phenomena

The excitonic emission from these NCs can be utilized in variety of different light emitting schemes such as photon down or upconversion, lasing and single-photon sources. Here we will discuss the underlying concepts and physics of variety emission schemes and some distinct phenomena only observed in perovskite NCs.

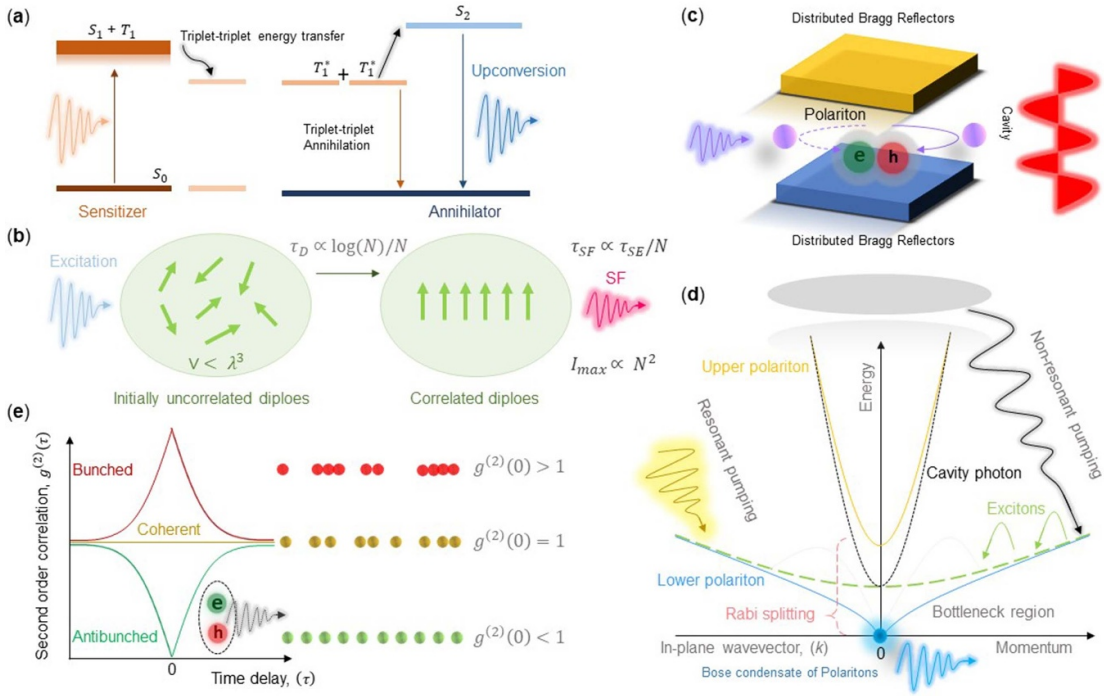

Figure 4. (a) Schematic of photon upconversion resulting from a triplet-triplet annihilation process. The sensitizer is excited yielding singlet (S_1) and triplet excitons (T_1). The triplet excitons are transferred to an 'annihilator' where there are able to diffuse and undergo fusion yielding a singlet (S_2) excited state of higher energy than the initial excitation wavelength. (b) Schematic of superfluorescence (SF) process where N initially uncorrelated states, within a volume (V) smaller than the excitation wavelength λ^3, are brought into phase through coupling to an electromagnetic field. τ_D, τ_{SF} and τ_{SE} are the coupling time, SF and spontaneous emission lifetimes. (c) Illustration of polariton coupling within the field between two distributed Bragg reflectors. (d) Illustration of dispersion branches formed when excitons strongly couple with cavity photons. Hot polaritons mostly populate the lower polariton branch undergoing cooling until the energy difference between photons and excitons is of the order of Rabi splitting, whereupon a condensate occurs as (at $k = 0$). Figure adapted from [76]. (e) Schematic of second order correlation, $g^{(2)}(\tau)$, for bunched (red), coherent (yellow) and antibunched (green) emission. Single photon emission occurs when $g^{(2)}(0) = 0$ with values below 1 having been reported for perovskite NCs [67, 68].

4.1. Up/down conversion and coherent/incoherent emission

Perovskite NCs when excited with x-rays may display x-ray excited optical luminescence (XEOL) [60]. The interaction of x-rays occurs primarily with the electrons of the constituent atoms and displays a linear attenuation coefficient that scales as $\sim Z^3$ (Z = atomic mass), and mass attenuation coefficient that scale as $\sim Z^4$, at energies up to ~100 keV [61]. As such the MHP NCs containing Pb offer a new family of scintillator materials with size tuneable XEOL. Upon x-ray excitation electrons are ejected from their electronic shell and subsequently secondary electrons are generated which then undergo thermalisation to produce a low energy band edge exciton, figure 3(b). Their emission can then be coupled with conventional photodetectors to detect the x-rays indirectly as scintillators. These NCs have already demonstrated superior performances than clinical x-ray imaging with a detection limit of ≈10 nGy s^{-1} [60]. The doping of perovskite NCs can also be undertaken, for example with rare-earth ions, to enable the tuning of energy transfer and characteristic emission. Figure 3(b) displays the XEOL obtained from $CsPbCl_3$:Tb^{3+} NCs. Here efficient quenching of the $CsPbCl_3$ NC emission (visible under 325 nm optical excitation) via energy transfer to the Tb^{3+} ion upon 30 keV x-ray excitation is demonstrated. Downconversion from $CsPbCl_3$:Yb^{3+} NCs with near-IR PLQY of ≈170% have also been demonstrated [62]. Here, a fast nonradiative energy transfer process is facilitated by defects induced by the dopant that results in excitation of two dopant ions while simultaneously quenching NCs band edge emission.

Alternatively, these NCs can also be used in photon upconversion schemes such as triplet–triplet annihilation, figure 4(a). In such a scheme, NCs are used as sensitizers along with an annihilator (emitter) which is typically chosen such that they have long triplet lifetimes which allows them to attain a sufficient concentration required for triplet–triplet collisional interactions. After the excitation of sensitizer the triplet exciton undergoes a triplet–triplet energy transfer process to an acceptor (Dexter-type non-radiative transfer) followed by exciton migration. When two migrating triplets collide they can annihilate (a spin allowed process) yielding a single higher energy excited singlet state. As this is an anti-Stokes process it is useful in many applications, however the overall process undergoes several losses and therefore the quantum yield is critical. Perovskite NCs have displayed a quantum yield of ≈10% for visible-to-ultraviolet upconversion

[63, 64]. Furthermore, they have been also employed as emitters in conjunction with lanthanides as sensitizers for near-infrared to NCs size dependent UV–vis emission. Here, the energy transfer occurs either via radiative photon reabsorption [65] or by Förster resonance energy transfer [66]. The latter requires a spectral overlap of sensitizer emission and emitters absorptions as well as a small spatial separation.

Superfluorescence (SF) is a many-body quantum phenomenon, that occurs when an ensemble of N incoherently excited states confined within a volume smaller than λ^3 (where, λ is the emission wavelength) spontaneously generates coherence (oscillating dipoles of N locked-in phase) via interaction with a common electromagnetic field [69, 70]. When this occurs, an intense coherent radiation-pulse is released with an accelerated radiative decay as, $\tau_{SF} \propto \tau_{SE}/N$ (where, τ_{SE} is the spontaneous emission decay time from uncoupled emitters and τ_{SF} is shortened SF decay time by the N emitters), figure 4(b). When coherent polarization is created by an external field (e.g. coherent laser) the phenomenon is referred to as the superirradiance (SR). Both eventuate only if the cooperative radiative decay time of the system becomes faster than the dephasing time of any other decoherence processes. Signature features of SF have been observed in densely packed superlattices of perovskites NCs [71] including an extremely narrow full-width at half-maximum ≈11 meV, red-shifted (≈70 meV) SF emission with a phase coherence time ≈140 fs, while the uncoupled NCs exhibit phase coherence time <40 fs. Although SF emission is found to occur only when high excitation fluence of ≈500 nJ cm^{-2} per pulse was used, with $\tau_{SF} \approx 150$ ps and $\tau_{SE} \approx 400$ ps.

Unlike SF and SR, amplified spontaneous emission (ASE) refers to the collective emission from a similar emitting system however fully incoherent. ASE is also observed in NCs even at a very low excitation threshold of ≈1–5 nJ cm^{-2} along with demonstration of lasing [72]. However, it is not yet clear though whether the ASE originates from single excitons [73], biexcitons [74] or by stimulated emission of free carriers [75].

4.2. Polariton lasing and single photon emission

Polariton based lasing at room temperatures is another distinct emission process displayed by these NCs along with the observation of the Rydberg exciton polaritons. Polariton emission is not only important from practical point of view as it does not require population inversion like convention lasing but also fundamentally because polaritons can form condensates—just like the Bose—Einstein condensates (non-equilibrium) that can be exploited to observe rich quantum phenomena. Polariton quasiparticles can be created by the strong coupling between the excitons and the photons within a microcavity. These particles have lifetimes shorter or comparable to crystal thermalization times ($\tau \approx 1$ ps) and a very light effective mass of ≈10^{-4} times of electron mass originating from their photonic constituent; and it is this aspect that makes them favourable to form condensates due de Broglie wavelength (λ_B) dependence on mass. Bose–Einstein condensates can occur above a certain threshold density of polaritons (when $\lambda_B \approx$ their average separation) or below a critical temperature (T). For an ideal Bose gas, this happens when $n{\lambda_B}^3 = 2.62$, where n is the boson density and $\lambda_B = \sqrt{2\pi\hbar/mk_BT}$, here m is the boson mass, $\hbar$ is reduced Plank's constant and k_B is the Boltzmann's constant [76]. Typically, such polariton condensates or lasing is achieved by sandwiching inorganic (e.g. quantum wells) or organic semiconductor (e.g. anthracene) between two distributed Bragg reflectors (DBRs), figure 4(c), and a similar configuration has been applied using perovskite films and NPs [77–80]. Since the nature of exciton is different in both classes of materials, they both have some drawbacks. In the case of inorganic Wannier–Mott excitons (small exciton binding energy which stems from their dielectric environment) polariton condensates are observed at low temperatures at densities lower than that of the exciton Mott or saturation density. While for organic materials this can be achieved at room temperature but the polariton-polariton Coulombic interaction (inherited from their excitonic constituents) is very weak for organic Frenkel excitons (large exciton binding energies). This hinders the polariton occupation of the ground state resulting in a much higher threshold density of polaritons being required. Perovskites, although inorganic, have a large exciton binding energy ($CsPbCl_3 \approx 75$ meV, $CsPbBr_3 \approx 40$ meV) [5], as well as large oscillator strength and short carrier lifetimes but still a typical threshold of ≈15 μJ cm^{-2} was required to observe polariton condensates.

After excitation by an external laser source, excitons strongly couple with cavity photons that results in formation of two dispersion branches—the lower and upper polaritons due to anti-crossing of exciton and photon dispersion, figure 4(d) [76]. The energy difference between these dispersions at zero in-plane momentum k is known as the Rabi splitting (≈10 meV for quantum wells) and its magnitude depends on the dipole coupling between them. Experimentally these dispersions can be observed via the k-space mappings of angle-resolved reflectivity or PL spectroscopy, however for perovskite NCs only the lower polaritons dispersion branch was observed possible due to large Rabi splitting ($CsPbCl_3 \approx 130$ meV and $CsPbBr_3 \approx 60$ meV). Even so, this provided a strong signature of polariton condensation in perovskite NCs. The hot polaritons mostly populate the lower polariton branch undergoing the cooling process until the energy difference between photons and excitons is of the order of Rabi splitting, figure 4(d). It is in this region that their condensate occurs as at this momentum ($k = 0$) their lifetime is reduced (less time is

available for cooling) and simultaneously the dispersion also steepens making them lighter. The polaritons decay (lifetimes $\tau \approx 1$–10 ps) by emitting photon through the mirrors that carries the same momentum and energy as that of the polaritons in the cavity. Their ground state emission emerges as blue shifted emission ($CsPbCl_3 \approx 90$ meV and $CsPbBr_3 \approx 60$ meV) from their exciton emission with a FWHM ≈ 10 meV that can become as narrow as $\approx$2 meV with the increase in pump intensity. Polariton lasing in NCs is further confirmed by inspecting long-range spatial coherence by measuring the first-order spatial correlation $\boldsymbol{g}^{(1)}(\boldsymbol{r}, -\boldsymbol{r}; \boldsymbol{\tau})$ or the phase coherence. Selective excitation of perovskite nanoplate revealed that these polariton condensates can also propagate up to a distance of 60 μm along the nanoplate, maintaining a long-range coherence with a group velocity of 10 μm ps^{-1}.

An even more intriguing aspect of MHPs is the observation of Rydberg exciton polaritons and their condensates which have not been observed in any semiconductors [80]. The underlying physics is same as that of polariton condensates, however, Rydberg exciton polaritons occur when the excitonic constituents of the polariton are in higher exciton states ($n > 2$). These excitonic states i.e. the ground and the first excited states ($n = 1$ and 2, hydrogen-like Rydberg series) are usually observable in the absorption spectrum of perovskites NCs, like many other NCs (e.g. CdSe), as they do not form a continuum but are rather typically energetically separated by about 1 eV because of the quantum confinement.

Another important application of perovskite NCs is their use as single-photon sources. The arrival of photons emitted from a source can be classified into three different categories as coherent, bunched or antibunched based on the statistical properties they follow, figure 4(e). In this regard, the nature of the emitted light can be distinguished and characterized by the degree of second order correlation, $\boldsymbol{g}^{(2)}(\boldsymbol{\tau})$. The photons associated with a perfectly coherent light arrive independently (unbunched) such that the $\boldsymbol{g}^{(2)}(\boldsymbol{\tau}) = 1$ for all time delays (τ) and for the bunched light $\boldsymbol{g}^{(2)}(\boldsymbol{\tau}) > 1$. Unlike these two, antibunching is non-classical and can only be explained by the quantum theory of light. For an antibunched light, $\boldsymbol{g}^{(2)}(\boldsymbol{\tau}) < 1$ (photons are separated in time) or otherwise the slope of $\boldsymbol{g}^{(2)}(\boldsymbol{\tau})$ at $\tau = 0$ is positive. For an ideal single-photon source $\boldsymbol{g}^{(2)}(0) = 0$ signifying that the probability of multiphoton emission event is zero [81]. Strong antibunching, which is signature of single-photon emission, has been observed in a single mixed-halide $CsPb(Cl/Br)_3$ perovskite NC with a $\boldsymbol{g}^{(2)}(0) = 0.3$ [67] and in a single $CsPbI_3$ NC PL at room temperatures with a $\boldsymbol{g}^{(2)}(0) = 0.05$ without any spectral filtering [68]. In NCs, the origin of single-photon emission is typically attributed to suppression of multi-photon or higher order radiative emission by an efficient and fast non-radiative Auger recombination. In experiments where high yields of biexciton emission is observed additional filtering is used to select only the exciton zero-phonon line. The optical coherence time ($\boldsymbol{T}_2$) of this zero-phonon line was found to be $\approx$80 ps which is a sizeable fraction of NCs spontaneous radiative lifetime ($\boldsymbol{T}_1$) $\approx$ 210 ps. Both are important parameters for evaluating NCs performance as a quantum emitter, as for an ideal emitter there is no dephasing of emitted photons i.e. $2\boldsymbol{T}_1/\boldsymbol{T}_2 = 1$. For perovskite NCs, a value of 5.4 have been observed for this ratio which in comparison is higher than that of epitaxially grown quantum dots (InAs $\approx$ 1.5) [82].

Although perovskite NCs have been demonstrated as coherent single-photon sources, multiexciton events and PL blinking (random fluctuations) that may arise in NCs charging/discharging must be suppressed.

5. Outlook

Research in perovskites will continue to increase towards more stable and environmentally friendly compositions, probably by new or improved synthetic methods, prompting more applications. NCs with reduced dimensions, such as assembled 2D perovskite heterostructures, are a particularly promising avenue. They combine the benefits of strongly size tuneable properties via significant quantum confinement, reduced density of surface traps via effective passivation, and enhanced radiative recombination rate via efficient energy funnelling. New studies on MEG in perovskites NCs will also continue to emerge and extend to these novel geometries and compositions. Improved structural stability and control over surface chemistry will not only result in more efficient and long-lasting devices but also allow for more detailed studies of the exciton dynamics in NCs of different sizes, shapes and compositions. Better understanding of these dynamics and effects will bring closer the realisation of efficient commercial devices based on perovskite NCs. The enhanced structural stability, particularly of the MHP systems, has opened up a new route to realising a new generation of x-ray detectors, with NCs demonstrating significant promise as scintillator materials.

The detailed study of excitonic states in perovskite NCs, and their control, has also demonstrated that they can display enhanced quantum behaviour. This is manifested in a multifold of ways including an enhanced Rashba effect, SF, polariton lasing, Rydberg exciton polariton condensates, and antibunched single photon emission. Though some of these effects remain observed within perovskite films, their study in NCs though technically challenging is an exciting opportunity. These studies to date have relied on optical excitation of the systems under study. Future technologies will demand electrical excitation which will

present further complexity due to the interaction of injected charge carriers with excited charge carriers and states. This will dramatically modify the dynamics of charge relaxation and the stability of excited states such as excitons, and in many cases is likely to lead to their rapid quenching or strong polaron effects dominating, especially as high injected carrier densities. As such hybrid systems where efficient resonant energy transfer from a host to perovskite are likely to be explored to overcome these.

Acknowledgment

Y J acknowledges the support of a PhD scholarship from Photon Science Institute, University of Manchester.

ORCID iDs

Ruben Ahumada-Lazo https://orcid.org/0000-0002-1524-9576
Maria-Eleni Kyriazi https://orcid.org/0000-0002-1427-0349
Antonios G Kanaras https://orcid.org/0000-0002-9847-6706
David Binks https://orcid.org/0000-0002-9102-0941
Richard J Curry https://orcid.org/0000-0001-8859-5210

References

[1] Buriak J M, Kamat P V, Schanze K S, Alivisatos A P, Murphy C J, Schatz G C, Scholes G D, Stang P J and Weiss P S 2017 *Chem. Mater.* **29** 8915–7
[2] Shamsi J, Urban A S, Imran M, De Trizio L and Manna L 2019 *Chem. Rev.* **119** 3296–348
[3] Akkerman Q A, Rainò G, Kovalenko M V and Manna L 2018 *Nat. Mater.* **17** 394–405
[4] Schmidt L C, Pertegás A, González-Carrero S, Malinkiewicz O, Agouram S, Espallargas G M, Bolink H J, Galian R E and Pérez-Prieto J 2014 *J. Am. Chem. Soc.* **136** 850–3
[5] Protesescu L, Yakunin S, Bodnarchuk M I, Krieg F, Caputo R, Hendon C H, Yang R X, Walsh A and Kovalenk M V 2015 *Nano Lett.* **15** 3692–6
[6] Gonzalez-Carrero S, Galian R E and Pérez-Prieto J 2015 *J. Mater. Chem.* A **3** 9187–93
[7] Lu P, Lu M, Wang H, Sui N, Shi Z, Yu W W and Zhang Y 2019 *InfoMat* **1** 430–59
[8] Sanehira E M, Marshall A R, Christians J A, Harvey S P, Ciesielski P N, Wheeler L M, Schulz P, Lin L Y, Beard M C and Luther J M 2017 *Sci. Adv.* **3** eaao4204
[9] Zhang L *et al* 2017 *Nat. Commun.* **8** 1–8
[10] Gong M, Sakidja R, Goul R, Ewing D, Casper M, Stramel A, Elliot A and Wu J Z 2019 *ACS Nano* **13** 1772–83
[11] Mondal N, De A, Das S, Paul S and Samanta A 2019 *Nanoscale* **11** 9796–818
[12] Makarov N S, Guo S, Isaienko O, Liu W, Robel I and Klimov V I 2016 *Nano Lett.* **16** 2349–62
[13] Chen J, Messing M E, Zheng K and Pullerits T 2019 *J. Am. Chem. Soc.* **141** 3532–40
[14] Griffiths J T *et al* 2019 *ACS Appl. Energy Mater.* **2** 6998–7004
[15] Castañeda J A, Nagamine G, Yassitepe E, Bonato L G, Voznyy O, Hoogland S, Nogueira A F, Sargent E H, Cruz C H B and Padilha L A 2016 *ACS Nano* **10** 8603–9
[16] Shukla A, Kaur Babu K J, Ghorai N, Goswami T, Kaur A and Ghosh H N 2020 *J. Phys. Chem. Lett.* **11** 6344–52
[17] Weidman M C, Goodman A J and Tisdale W A 2017 *Chem. Mater.* **29** 5019–30
[18] Etgar L 2018 *Energy Environ. Sci.* **11** 234–42
[19] Polavarapu L, Nickel B, Feldmann J and Urban A S 2017 *Adv. Energy Mater.* **7** 1–9
[20] Li Y, Luo X, Ding T, Lu X and Wu K 2020 *Angew. Chem., Int. Ed.* **59** 14292–5
[21] Dong Y *et al* 2020 *Nat. Nanotechnol.* **15** 668–74
[22] Saidaminov M I, Mohammed O F and Bakr O M 2017 *ACS Energy Lett.* **2** 889–96
[23] Beard M C, Midgett A G, Hanna M C, Luther J M, Hughes B K and Nozik A J 2010 *Nano Lett.* **10** 3019–27
[24] Schaller R D and Klimov V I 2004 *Phys. Rev. Lett.* **92** 1–4
[25] Klimov V I 2007 *Annu. Rev. Phys. Chem.* **58** 635–73
[26] Nozik A J 2008 *Chem. Phys. Lett.* **457** 3–11
[27] Beard M C and Ellingson R J 2008 *Laser Photon. Rev.* **2** 377–99
[28] Binks D J 2011 *Phys. Chem. Chem. Phys.* **13** 12693–704
[29] Shockley W and Queisser H J 1961 *J. Phys. D: Appl. Phys.* **32** 510–9
[30] Smith C and Binks D 2014 *Nanomaterials* **4** 19–45
[31] Forgacs D, Wojciechowski K and Malinkiewicz O 2020 Perovskite Photovoltaics: From Laboratory to Industry ed V Petrova-Koch, R Hezel and A Goetzberger (Cham: Springer International Publishing) pp 219–55
[32] Schaller R D, Pietryga J M and Klimovm V I 2007 *Nano Lett.* **7** 3469–76
[33] Li M, Begum R, Fu J, Xu Q, Koh T M, Veldhuis S A, Grätzel M, Mathews N, Mhaisalkar S and Sum T C 2018 *Nat. Commun.* **9** 3–9
[34] Zohar G, Baer R and Rabani E 2013 *J. Phys. Chem. Lett.* **4** 317–22
[35] De Weerd C *et al* 2018 *Nat. Commun.* **9** 1–9
[36] Cong M, Yang B, Chen J, Hong F, Yang S, Deng W and Han K 2020 *J. Phys. Chem. Lett.* **11** 1921–6
[37] Lei L *et al* 2020 *Adv. Mater.* **32** 1906571
[38] Bi C, Wang S, Kershaw S V, Zheng K, Pullerits T, Gaponenko S, Tian J and Rogach A L 2019 *Adv. Sci.* **6** 1900462
[39] Yuan M *et al* 2016 *Nat. Nanotechnol.* **11** 872–7
[40] Pan J *et al* 2019 *Angew. Chem.* **58** 1–6
[41] Becker M A *et al* 2018 *Nature* **553** 189–93
[42] Stranks S D and Plochocka P 2018 *Nat. Mater.* **17** 381–2

[43] Sercel P C, Lyons J L, Wickramaratne D, Vaxenburg R, Bernstein N and Efros A L 2019 *Nano Lett.* **10** 4068–77
[44] Fu M, Tamarat P, Huang H, Even J, Rogach A L and Lounis B 2017 *Nano Lett.* **17** 2895–901
[45] Isarov M, Tan L Z, Bodnarchuk M I, Kovalenko M V, Rappe A M and Lifshitz E 2017 *Nano Lett.* **17** 5020–6
[46] Canneson D, Shornikova E V, Yakovlev D R, Rogge T, Mitioglu A A, Ballottin M V, Christianen P C M, Lhuillier E, Bayer M and Biadala L 2017 *Nano Lett.* **17** 6177–83
[47] Tamarat P, Bodnarchuk M I, Trebbia J-B, Erni R, Kovalenko M V, Even J and Lounis B 2019 *Nat. Mater.* **18** 717–24
[48] Tamarat P, Hou L, Trebbia J-B, Swarnkar A, Biadala L, Louyer Y, Bodnarchuk M I, Kovalenko M V, Even J and Lounis B 2020 *Nat. Commun.* **11** 6001
[49] Saran R, Heuer-Jungemann A, Kanaras A G and Curry R J 2017 *Adv. Opt. Mater.* **5** 1700231
[50] Iaru C M, Geuchies J J, Koenraad P M, Vanmaekelbergh D and Silov A Y 2017 *ACS Nano* **11** 11024–30
[51] Ramade J *et al* 2018 *Appl. Phys. Lett.* **112** 072104
[52] Shinde A, Gahlaut R and Mahamuni S 2017 *J. Phys. Chem.* C **121** 14872–8
[53] Butkus J, Vashishtha P, Chen K, Gallaher J K, Prasad S K K, Metin D Z, Laufersky G, Gaston N, Halpert J E and Hodgkiss J M 2017 *Chem. Mater.* **29** 3644–52
[54] Zhao W, Qin Z, Zhang C, Wang G, Dai X and Xiao M 2019 *Appl. Phys. Lett.* **115** 243101
[55] Diroll B T, Nedelcu G, Kovalenko M V and Schaller R D 2017 *Adv. Funct. Mater.* **27** 1606750
[56] Liu A, Bonato L G, Sessa F, Almeida D B, Isele E, Nagamine G, Zagonel L F, Nogueira A F, Padilha L A and Cundiff S T 2019 *J. Chem. Phys.* **151** 191103
[57] Mondal A, Aneesh J, Ravi V K, Sharma R, Mir W J, Beard M C, Nag A and Adarsh K V 2018 *Phys. Rev.* B **98** 115418
[58] Francisco-López A, Charles B, Weber O J, Alonso M I, Garriga M, Campoy-Quiles M, Weller M T and Goñi A R 2019 *Phys. Chem. Lett.* **2019** 2971–7
[59] Rubino A, Francisco-López A, Barker A J, Petrozza A, Calvo M E, Goñi A R and Míguez H 2021 *J. Phys. Chem. Lett.* **12** 569–75
[60] Chen Q *et al* 2018 *Nature* **561** 88–93
[61] Boone J M 2000 X-ray production, interaction, and detection in diagnostic imaging *Handbook of Medical Imaging* (*Physics and Psychophysics*, vol 1) ed R L Van Metter, J Beutel and H L Kundel (Bellingham: SPIE Press) ch 1
[62] Milstein T J, Kroupa D M and Gamelin D R 2018 *Nano Lett.* **18** 3792–9
[63] He S, Luo X, Liu X, Li Y and Wu K 2019 *J. Phys. Chem. Lett.* **10** 5036–40
[64] Mase K, Okumura K, Yanai N and Kimizuka N 2017 *Chem. Commun.* **53** 8261–4
[65] Zheng W, Huang P, Gong Z, Tu D, Xu J, Zou Q, Li R, You W, Bünzli J C G and Chen X 2018 *Nat. Commun.* **9** 3462
[66] Zeng M, Singh S, Hens Z, Liu J, Artizzu F and Deun R V 2019 *J. Mater. Chem.* C **7** 2014–21
[67] Rainò G, Nedelcu G, Protesescu L, Bodnarchuk M I, Kovalenko M V, Mahrt R F and Stöferle T 2016 *ACS Nano* **10** 2485–90
[68] Park Y-S, Guo S, Makarov N S and Klimov V I 2015 *ACS Nano* **9** 10386–93
[69] Dicke R H 1954 *Phys. Rev.* **93** 99
[70] Cong K, Zhang Q, Wang Y, Noe G T, Belyanin A and Kono J 2016 *J. Opt. Soc. Am.* B **33** C80–101
[71] Rainò G, Becker M A, Bodnarchuk M I, Mahrt R F, Kovalenko M V and Stöferle T 2018 *Nature* **563** 671–5
[72] Yakunin S, Protesescu L, Krieg F, Bodnarchuk M I, Nedelcu G, Humer M, Luca G D, Fiebig M, Heiss W and Kovalenko M V 2015 *Nat. Commun.* **6** 8056
[73] Navarro-Arenas J, Suárez I, Chirvony V S, Gualdrón-Reyes A F, Mora-Seró I and Martínez-Pastor J 2019 *J. Phys. Chem. Lett.* **10** 6389–98
[74] Nagamine G, Rocha J O, Bonato L G, Nogueira A F, Zaharieva Z, Watt A A R, Cruz C H, Brito D and Padilha L A 2018 *J. Phys. Chem. Lett.* **9** 3478–84
[75] Geiregat P, Maes J, Chen K, Drijvers E, De Roo J, Hodgkiss J M and Hens Z 2018 *ACS Nano* **12** 10178–88
[76] Byrnes T, Kim N Y and Yamamoto Y 2014 *Nat. Phys.* **10** 803–13
[77] Su R, Ghosh S, Wang J, Liu S, Diederichs C, Liew T C H and Xiong Q 2020 *Nat. Phys.* **16** 301–6
[78] Su R, Diederichs C, Wang J, Liew T C H, Zhao J, Liu S, Xu W, Chen Z and Xiong Q 2017 *Nano Lett.* **17** 3982–8
[79] Su R, Wang J, Zhao J, Xing J, Zhaon W, Diederichs C, Liew T C H and Xiong Q 2018 *Sci. Adv.* **4** eaau0244
[80] Bao W *et al* 2019 *Proc. Natl Acad. Sci.* **116** 20274–9
[81] Chunnilall C J, Degiovanni I P, Kück S, Müller I and Sinclair A G 2014 *Opt. Eng.* **53** 081910
[82] Utzat H *et al* 2019 *Science* **363** 1068–72